Available online at www.sciencedirect.com
ScienceDirect
Acta Materialia 59 (2011) 914–926
Acta MATERIALIA
www.elsevier.com/locate/actamat

Interaction of liquid and solid gallium with thin silver films: Synchronized spreading and penetration

Evgeny Glickman [a,*], Mario Levenshtein [b], Lior Budic [b], Noam Eliaz [b]

[a] School of Electrical Engineering, Tel Aviv University, Ramat Aviv, Tel Aviv 69978, Israel
[b] School of Mechanical Engineering, Tel Aviv University, Ramat Aviv, Tel Aviv 69978, Israel

Received 6 July 2010; received in revised form 30 August 2010; accepted 2 October 2010
Available online 9 November 2010

Abstract

The synchronized lateral spreading and through-penetration of liquid and solid gallium (Ga) in supported thin polycrystalline films of silver (Ag) were studied. The spreading and penetration kinetics were presumably controlled by a common mechanism. The spreading rate in the 0.5 μm thick film was found to be constant with time. The activation energies of the process responsible for spreading/penetration of liquid and solid Ga were $E_L \approx 28.9 \pm 4.8$ kJ mol^{-1} and $E_S \approx 48.2 \pm 9.6$ kJ mol^{-1}, respectively. Grain boundary grooving, with Ag diffusion out of the groove either through liquid Ga or through solid Ga, was suggested as a possible mechanism of the spreading and penetration. The model proposed reproduced the observed spreading/penetration rates and gave reasonable estimates of the energies E_S and E_L.
© 2010 Acta Materialia Inc. Published by Elsevier Ltd. All rights reserved.

Keywords: Gallium; Silver; Thin films; Grain boundary diffusion; Wetting

1. Introduction

The terms grain boundary wetting (GBW) and grain boundary penetration (GBP) refer to the formation and extension of capillary liquid–metal films, grooves or channels along grain boundaries (GBs) in solid metals [1–4]. In contrast to liquid–metal (LM) embrittlement, GBW was observed in many metals in the absence of applied stress [1–6]. GBW represents a kind of intergranular corrosion in liquid metals and may be attributed to dissolution and fast out-of-tip diffusion of solid metal atoms through the LM channels. It is well known that the diffusion coefficient in liquid metals, D_L, is faster by at least three orders of magnitude than in solid metals ($D_L \approx 10^{-9}$ m^2 s^{-1} vs. $D_S \approx 10^{-12}$ m^2 s^{-1}), even around the melting point T_m, while for $T < T_m$ the difference can reach many orders of magnitude, the more so the lower the temperature is. Hence, GBW can be fast and can thus lead to fast degradation of mechanical properties, thermal conductivity and electrical conductivity of the solid metal.

The kinetic mechanism of GBP/GBW is not yet clear. It has been proposed to relate either to fast diffusion-assisted mass transport in liquid stimulated by capillary stresses [5,7], coherent [8] or residual [9] internal stresses, to solid-state self-diffusion [1] or hetero-diffusion [10] into GBs. The rate of GBW/GBP is typically of the order of 1–10 μm s^{-1} [1], which suggests that GBP might cause a grave reliability problem for microelectronic thin films, e.g. contact pads, multilayer under-ball metallurgies and solder barrier layers, which have typically sub-micrometer thickness and experience intimate contact with LMs in the process of soldering. This problem can well be of paramount importance with the transition to lead-free solder alloys, which interaction with GB in thin-film metals occurs at higher reflow temperature of ~240 °C for about 10 s [11].

In general, very little has been published so far in the area of GBW in thin metal films. Furthermore, even for bulk metals, most GBW studies have been performed on simple eutectic systems, while all real solder alloys form

* Corresponding author. Tel.: +972 3 6407352; fax: +972 3 6423508.
E-mail address: evgeny@eng.tau.ac.il (E. Glickman).

1359-6454/$36.00 © 2010 Acta Materialia Inc. Published by Elsevier Ltd. All rights reserved.
doi:10.1016/j.actamat.2010.10.004

intermetallic compounds (IMCs) with thin film microelectronic metals. The competition between IMC formation and dissolution rates in this case becomes the critical issue [11,12].

The objective of this work was to study the kinetics and mechanism of surface spreading and through-penetration of liquid and solid Ga in supported thin films of polycrystalline silver. The Ag–Ga phase diagram is presented in Fig. 1 [13,14]. The diagram shows Ga–Ag eutectic ($L \leftrightarrow Ag_3Ga_2 + Ga$) at 99.98 at.% Ga and $T = 29$ °C, very close to the melting point of Ga ($T_m(Ga) \approx 29.8$ °C), and IMCs (ζ, ζ' and Ag_3Ga_2) in ranging from 22.1 to 40 at.% Ga. The solubility limit of Ga in solid Ag at room temperature (RT) is $C_{\infty S} = 11$ at.% [14], whereas the solubility $C_{\infty L}$ of Ag in liquid Ga is lower than 1 at.% between 30 and 60 °C, the latter being the maximal temperature used in our spreading experiments. The equilibrium solubility $C_{\infty,Ag/Ga}$ of Ag in solid Ga is not known; extrapolation of the liquidus line shown in Ref. [15] yields a rough upper estimate of $C_{\infty,Ag/Ga} \approx 1$ at.%.

Along with the presence of IMCs formed by Ga with Ag, the important reason for selection of Ag–Ga system for investigation of GB penetration and spreading is that Ga is remarkably prone to undercooling and can remain liquid for quite a long time even at a temperature of about −10 °C, which is 40 °C below its melting point. This specific property of liquid Ga was confirmed recently by Koizumi et al. [16–18] by use of ultrasonic attenuation measurements in an "Al thin film–Ga" system [16]. The wide temperature range of existence of the liquid phase enabled measurements of the GBP rate of Ga across a wide temperature range, thus allowing reliable data on the activation energy of the process to be acquired. Furthermore, the tendency for large Ga undercooling provided an interesting opportunity for comparison between the GBP/spreading kinetics of heavily supercooled, but still liquid, Ga with the kinetics observed for solid Ga at the same temperature, $T < T_m(Ga)$. This opportunity could help clarify the underlying mechanism of GBP. Additional advantages of the selected system Ag–Ga are: (i) low resistivity Ag is a promising thin-film interconnect material for microelectronics; (ii) Ag is a noble metal, thus there is no need for protective atmosphere to prevent its oxidation during the experiments at around RT; and (iii) Ga has a low vapor saturation pressure and thus does not contaminate the equipment.

2. Experimental

A 5 N (99.999%) Ag target was used for vacuum ion-sputtering deposition of Ag films on 1 mm thick transparent Corning glass substrates. The films had a thickness $h = 0.47$ μm, making them non-transparent to visible light. The grain size $d \approx 0.1$–0.2 μm of the polycrystalline film was measured by atomic force microscopy (AFM). Prior to exposure to Ga, the surface of the Ag film was rinsed with distilled water, acetone and isopropanol, and subsequently dried with pure Ar gas. The Ga was melted by hot air, and small drops of it, with varying initial sizes, were carefully placed on the Ag film.

In order to avoid massive dissolution of the Ag film in Ga, we used drops of liquid Ga that were presaturated, prior to the wetting experiments, with Ag – up to the solubility limit $C_{\infty,Ga/Ag}$ of ~3 at.% Ag and even contained some excessive Ag in precipitates. This was done by heating a small volume of Ga together with small chips of Ag (total ~20 at.% Ga) for 3–4 h at 200 °C. The presence of Ag-rich precipitates in liquid Ga formed a large Ag reservoir, which guaranteed that the liquid was saturated with Ag, even at the highest temperature of 60 °C used in our experiments.

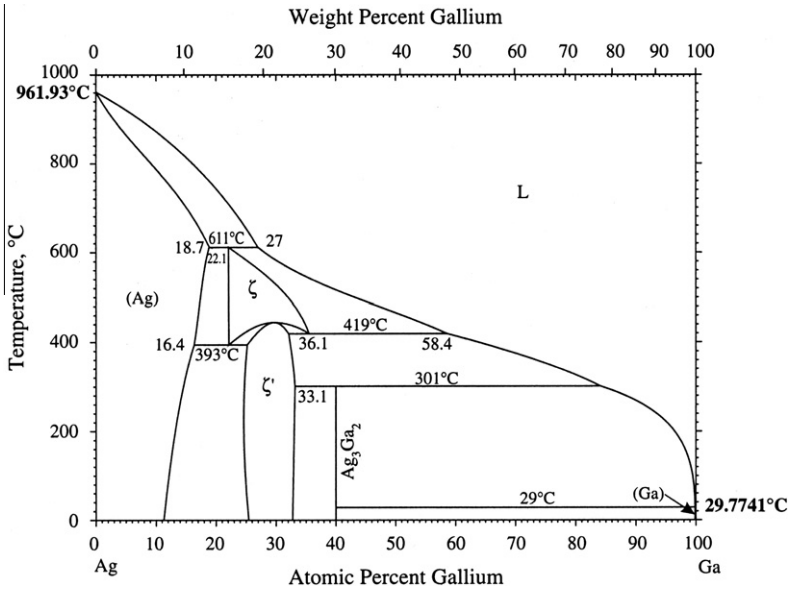

Fig. 1. The silver–gallium binary phase diagram [13,14].

As Ga is apt to undercooling well below its equilibrium melting point, the Ga drops could be maintained at $T < T_m(\mathrm{Ga})$. Alternatively, the drops were kept solid at the same exposure temperature via precooling in a mixture of liquid acetone and dry ice, having a temperature of about −78 °C, and subsequently heating them to a specific temperature below $T_m(\mathrm{Ga})$. This heating was done either in a freezer/refrigerator or in a furnace. All wetting/penetration experiments were performed in ambient air.

Bottom view (i.e. through the glass) and top view light photomicrographs were acquired to trace the morphology and velocity $v = \Delta R/\Delta t$ of the Ga wetting front between +60 and −10 °C. Here, R is the radius of the spreading drop of Ga and t is time. This was done by means of an Olympus IX71 light microscope, equipped with ColorView II CCD camera and analySIS docu software package, both from Soft Imaging System. Scanning electron microscopy (SEM) and AFM were used to characterize the surface morphology, while energy dispersive X-ray spectroscopy (EDS) was used to determine the chemical composition in different regions of the surface. The contact mode AFM work was done in air, using a PicoSPM™ microscope and tips made of Si_3N_4 (from Veeco), having a spring constant of 0.12 N m^{-1}.

3. Results

The bottom-view microscope images revealed the first signs of Ga penetration through the Ag film after exposure for about 25 s. Subsequently, spreading by radial extension of a lusterless "grey" region around a "black" region of the drop itself became evident (Fig. 2). The area A_d of the black region and its shape did not change with time. It was remarkable to see that at any moment, for different temperatures and drop sizes, the shape of the spreading front as seen from the bottom was nearly an exact mirror reflection of the corresponding top view (Fig. 3). As the Ag film was opaque to visible light, this observation suggests a common mechanism that controlled both the surface spreading of Ga and its penetration through the thin Ag film.

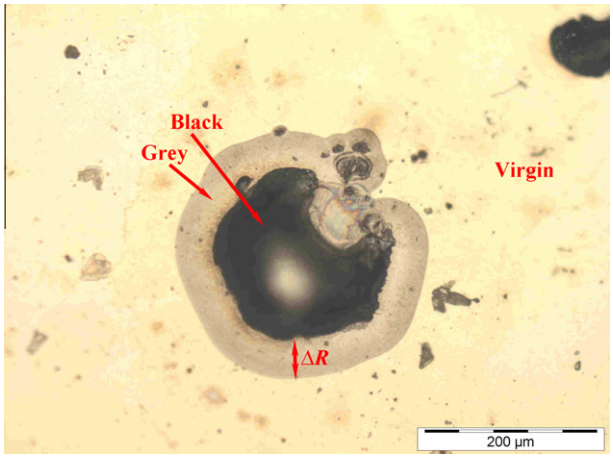

Fig. 2. Top-view light photomicrograph of a Ga drop on the surface of a 0.47 μm thick, opaque polycrystalline Ag film supported by transparent glass. This image shows a lusterless "grey" region that spreads at room temperature with a constant linear velocity $v = \Delta R/\Delta t$, as well as the "black" region of the Ga drop and a "virgin" region of the intact Ag film.

Cross-sections were prepared by placing a few Ga drops on the Ag film, as close as possible to each other. The Ga/Ag/glass "sandwich" was then frozen at $T = -78$ °C and subsequently fractured by bending. SEM images of the cross-sections showed that the Ga drops rested on the Ag surface with the contact (wetting) angle $\theta \approx 30°$ (Fig. 4a). The contrast of the Ag film beneath the Ga drop is evident in Fig. 4a. The presence of the Ag film is also evident from the EDS line scans (Fig. 4b). It was concluded that the Ag film beneath the Ga drop did not dissolve during the experiment and therefore the good matching between the bottom- and top-view images reflected the penetration of Ga through the solid Ag film but not the two sides of the liquid Ga drop.

SEM/EDS and X-ray mapping enabled us to relate the visually different regions at the surface of the film (Fig. 5) to different chemical compositions, as given below in at.%:

(1) The virgin Ag region ahead of the spreading grey front: 90 Ag, 2 Ga, 8 Si (the latter – from the glass substrate, while small Ga signal comes likely from the parasite scattering).
(2) The grey region: 60 Ag, 35 Ga, 5 Si. The fact that EDS shows Si from the glass substrate means that the depth of the EDS analysis (~1 μm) exceeds not only the thickness of the liquid Ga-rich layer, but also the total thickness of the Ga and 0.47 μm Ag layers. This implies that the actual Ga concentration in the Ga-rich grey region may be considerably larger compared to the measured 35 at.% and, therefore, that the spreading grey layer possibly represents a mixture of IMCs and liquid Ga.
(3) The black region, closer to the perimeter of the drop: 92–96 Ga, 8–4 Ag.
(4) The black region, at the center of the drop: 99 Ga, 1 Ag.
(5) Both the SEM images and the EDS data show distinct borders between the three regions (Fig. 5a), and a sharp contrast between Ga concentrations in the regions (Fig. 5b). These findings suggest that Ga spreading over the grey region did not occur by surface diffusion; if the latter was the case, the Ga concentration profile would have been smoother. On the other hand, the fact that the black region did not expand with time indicates that the spreading mechanism cannot be simplified to flow of bulk liquid phase.

AFM clearly revealed the original grain size in the virgin area, $d \approx 0.1$–0.2 μm (Fig. 6a), while the grain structure within the grey area was much less pronounced (Fig. 6b). The structure observed here has a smooth contour that

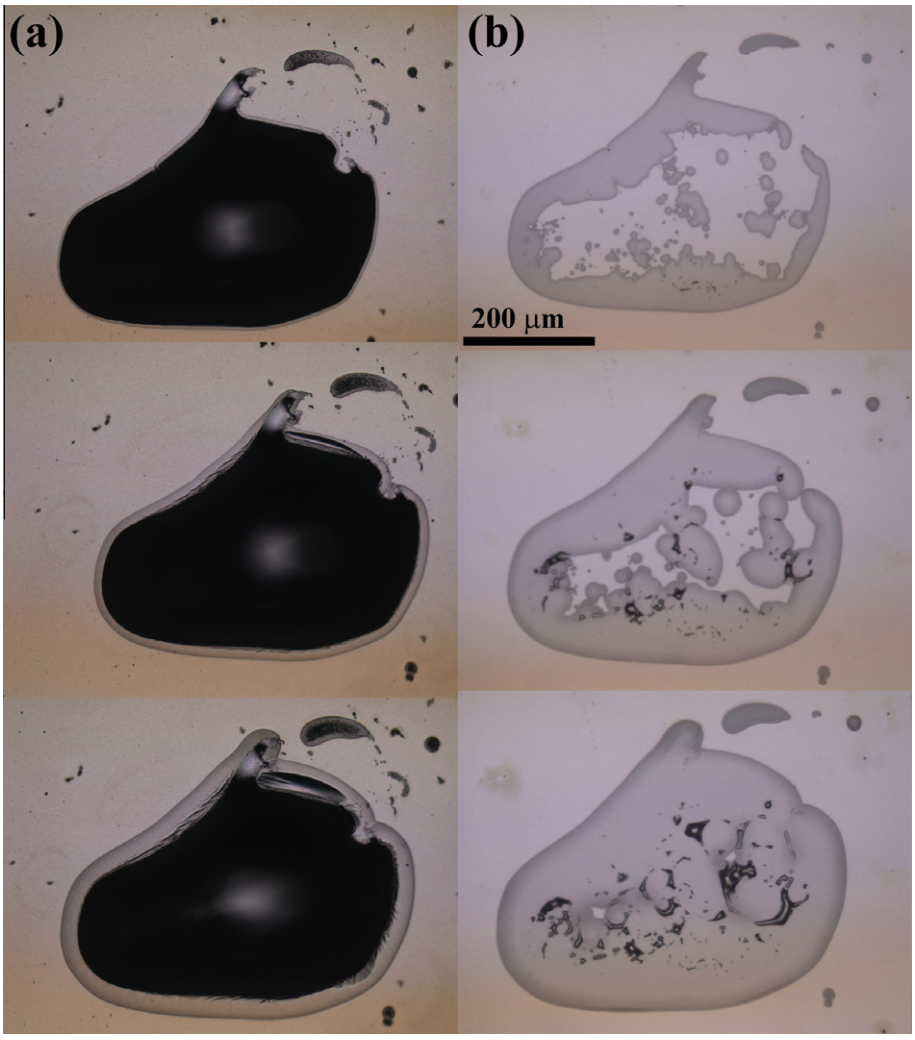

Fig. 3. Perfect correspondence between the top view (a) and the bottom view (b) of a Ga drop spreading at room temperature over the surface of a 0.47 μm thick, opaque polycrystalline Ag film on transparent glass. The images were acquired at 1 min (top), 90 min (middle) and 200 min (bottom) after Ga deposition. Continuous spreading of the grey area around the drop is clearly evident.

suggests a wetted surface, which can be attributed to the presence of liquid Ga, which filled the grooves between the grains and caused fast liquid-phase-assisted mass transport from the ridges to valleys; the latter process additionally favors smoothening. Formation of very large, elongated grains on the micrometer length was observed at the interface between the grey and virgin regions (Fig. 6c). This observation is compatible with the suggested presence of liquid Ga in the GB grooves, and can presumably be interpreted as the result of the well-known phenomenon of liquid-phase-assisted coarsening/sintering/recrystallization of metals [19]. The observed formation of whiskers at the moving front (Fig. 6f) reflects likely a relief of compressive stresses, which form in the Ag film due to volumetric changes caused by interdiffusion of Ga and IMC formation. The presence of a wetting liquid phase was reported to favor whisker morphology with a high aspect ratio by "activating" the growing tip; this effect is explored in the vapor–liquid–solid process of crystal growth [20]. All these findings show that a thin film/precursor film formed in the grey region ahead of the drop. The thickness of this film (averaged over the green line of length ~100 μm in Fig. 6d and e) is about 150 nm. The observed smoothed surface contour (Fig. 6b), together with the microstructure coarsening (Fig. 6c), suggests the presence of a liquid phase at the moving front of the precursor region, which also contains IMCs formed between Ga and Ag. Fig. 6e shows a well-defined hump of height ~250 nm and about the same width at the moving front of the precursor film. It is known that the wetting films can develop a hump at the end when the contact line cannot move as fast as the fluid being driven by the acting stresses [21,22]. Several factors can lead to such a situation, e.g. pinning of the triple line due to the ridging effect [23].

The first observation of a thin precursor film of liquid metal that extends a few hundred micrometers ahead of the macroscopic drop and has a hump at the edge was made by Saiz and Tomsia [22] for the fully miscible metal

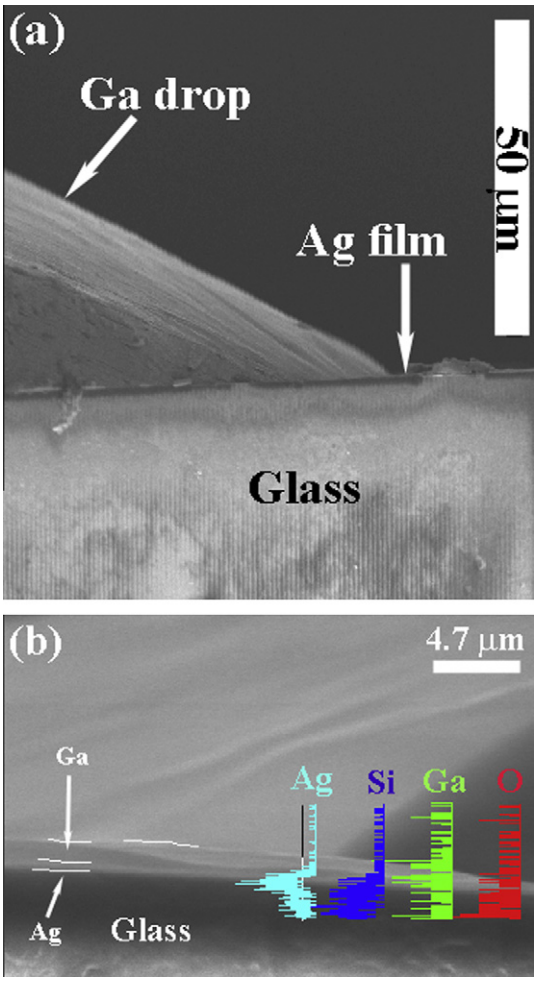

Fig. 4. (a) SEM image of the fracture surface of a frozen Ga drop, exposing the Ag film beneath it. (b) EDS line scans support the presence of the Ag film.

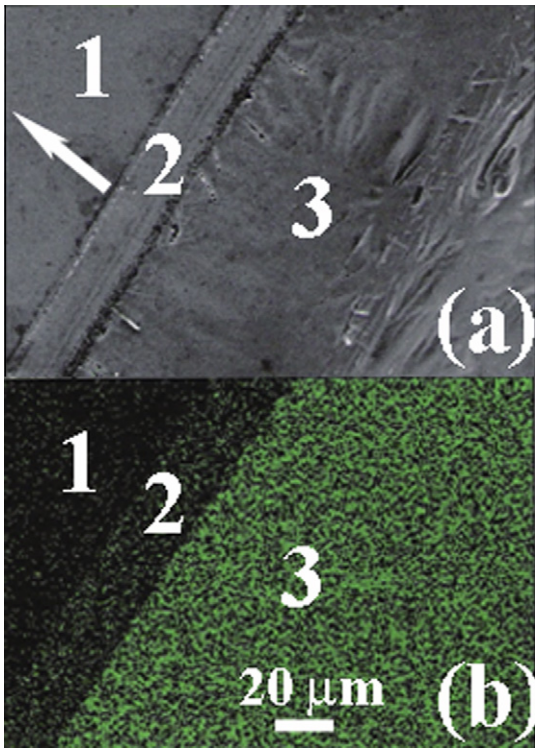

Fig. 5. Secondary electrons image (a) and X-ray spatial mapping of Ga (b), demonstrating the virgin (1), grey (2) and black (3) regions. The front of the grey region extends in the direction shown by arrow in (a).

system Au–Ni. The authors attributed their observations to the Marangoni stress associated with the gradient of liquid surface energy due to varying liquid composition under simultaneous spreading, dissolution and interdiffusion. Although our observations relate to the Ag–Ga system with limited mutual solubility and the existence of IMCs, the line scan height profile in Fig. 6e bears a striking resemblance to that reported in Fig. 4b in Ref. [22]. This may suggest that, in both cases, the hump results from the Marangoni stress, the formation of which does not necessarily require full miscibility of the liquid and substrate metals (in contrast to the idea expressed in Ref. [22]). Another possible explanation is given in Section 4.1, in terms of coupling between the interface reaction flux and the transport flux in the precursor film region. Additional work is required to select between these two possible explanations; at present, the second possibility seems more suitable because it fits better the wetting mechanism of spreading discussed in Section 4.1.

The time dependence of the drop area at RT is shown in Fig. 7a for four drops with different initial areas A_0 (17,300, 47,800, 107,370 and 116,010 μm^2). As mentioned before and illustrated in Fig. 7a for drop #3, the area of the black region did not change with time. In contrast, the area of the "grey" region ΔA grew linearly with time, showing a constant area spreading rate $S = \Delta A/\Delta t$, which increased with A_0 (see Fig. 7a). This behavior suggests that the spreading rate was controlled by the rate of interface "reactions" at the moving front (e.g. dissolution, movement of the ridges, GB grooving, IMC formation or other detachment/attachment events), rather than by diffusion transport or viscous flow, for which a square root time dependence is usually valid [24,25].

The spreading distance of the drop edge $\Delta R(t)$ in our experiments was always much smaller than the initial drop diameter $2R_0$, namely:

$$\Delta R(t) = [R(t) - R_0] \ll 2R_0 = (4A_0/\pi)^{1/2} \quad (1)$$

Assuming a circular drop, the increment in the drop area ΔA under the small-scale displacement condition expressed by Eq. (1) is:

$$\Delta A \approx 2\pi R_0 \Delta R(t) \quad (2)$$

For diffusion-controlled spreading regime $\Delta R \sim Dt^{1/2}$, the spreading rate $S = \Delta A/\Delta t$ in Fig. 7a should decrease with time. In contrast, for an interface reaction-controlled regime:

$$\Delta R(t) = \beta t \quad (3)$$

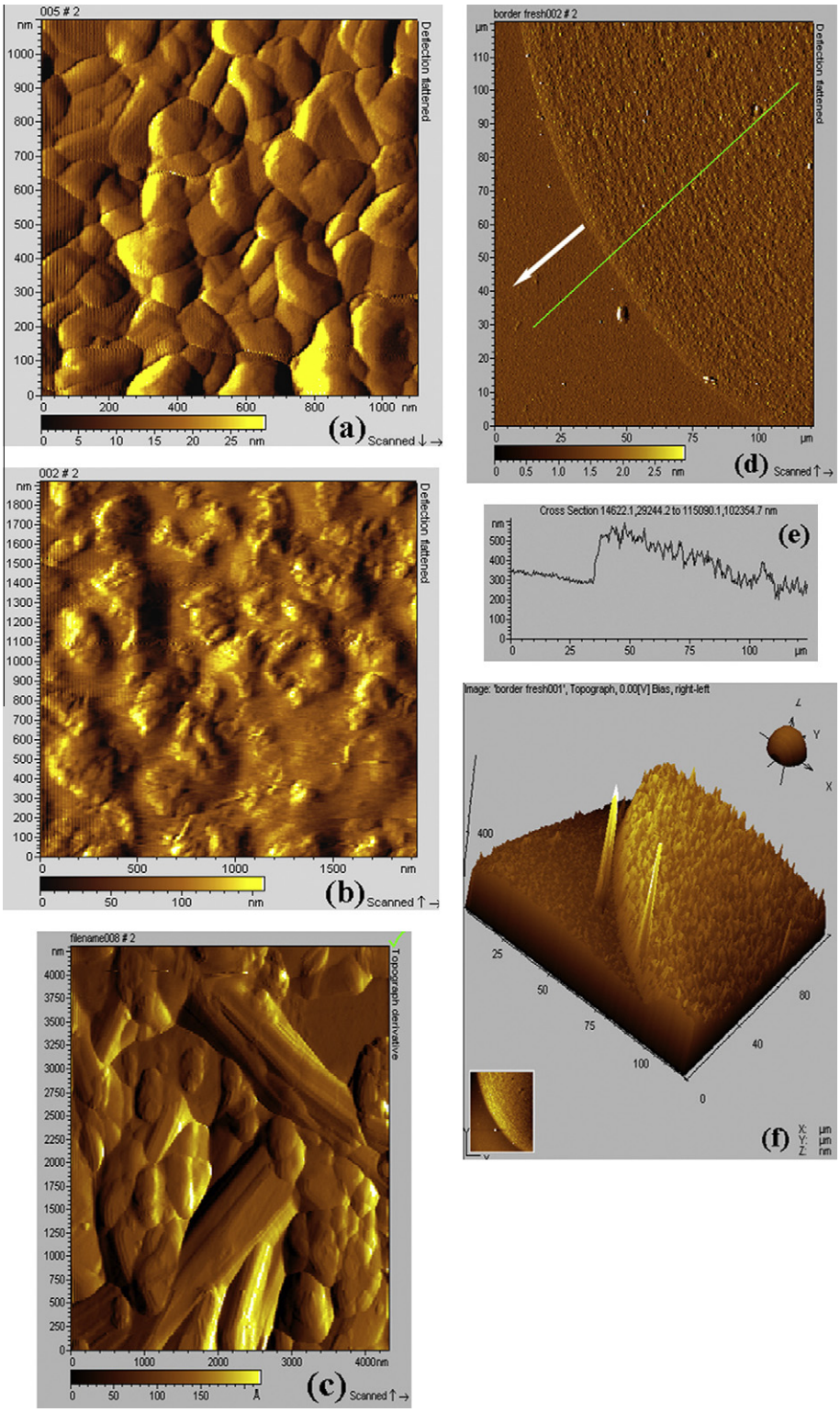

Fig. 6. AFM in situ observations: (a) microstructure of the virgin region; (b) smoothed microstructure in the grey region; (c) microstructure coarsening at the border between the grey and virgin regions; (d) front of the grey region that extends ahead of the drop at RT; (e) the height profile along the green line in (d); (f) 3-D view of the moving front: the grey region is on the right and the virgin region is on the left of the front.

where the kinetic coefficient β is determined by the rate of the reaction at the spreading front, has the meaning of a linear spreading rate, and should not depend on time. In this case:

$$\Delta A \approx 2\pi R_0 \beta t \tag{4}$$

and the spreading rate S should be constant in time:

$$S = \Delta A/\Delta t = 2\pi R_0 \beta \tag{5}$$

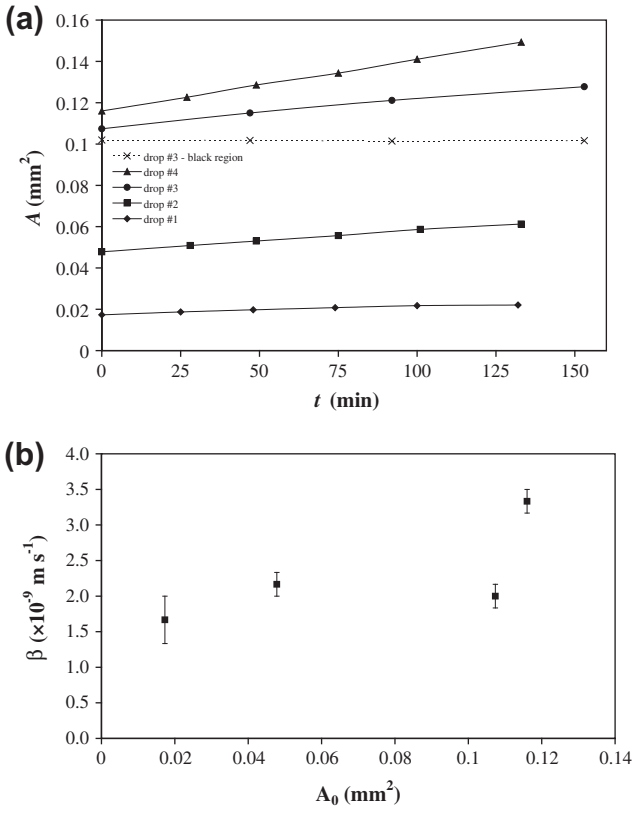

Fig. 7. Kinetics of Ga spreading on the surface of the 0.47 μm thick polycrystalline Ag film at RT (20 °C). (a) Linear time dependence of the drop area $A = A_0 + St$ for drops having different initial areas A_0 of the black region. (b) The kinetic coefficient $\beta = S/2\pi R_0$ does not depend on A_0 in a wide range of A_0 below ~110,000 μm^2.

Comparing the plots in Fig. 7a with Eqs. (2) and (5), we conclude that a parabolic diffusion regime, described by Eq. (2), does not match our experimental results obtained under small-displacement conditions $\Delta R(t) \ll 2R_0$, while the linear kinetic regime does. Indeed, Eq. (5) predicts a constant spreading rate S that increases with the initial drop size R_0, and the data in Fig. 7a are in a qualitative agreement with these predictions, showing that the slope S is actually constant and increases with the initial drop area A_0.

Fig. 7b was plotted based on the data in Fig. 7a. It shows that the kinetic coefficient β calculated from the experiment and Eq. (5) does not depend on A_0, at least in the wide interval of the initial drop areas 20,000 μm^2 < A_0 < 110,000 μm^2 that was mainly used in our further experiments.

So far, it has been assumed that the drops are circular, or close to circular, and spread uniformly in all directions. However, this assumption is not always true. Our observations revealed that Ga drops sometimes spread also in a "freak" way, exhibiting asymmetrical shapes (see Fig. 3) and outward movement of only part of their perimeter (Fig. 8). In these cases, the liner displacement ΔR was measured directly at four or five different points across the perimeter of the drop, and the average $\Delta\bar{R}(t)$ was then

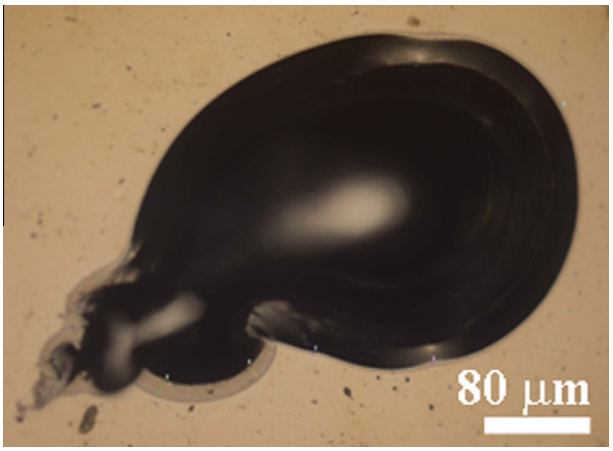

Fig. 8. Example of a non-circular drop for which Ga spreading occurs only across part of the drop perimeter.

calculated. When plotting the measured linear spreading rate $\Delta\bar{R}/\Delta t$ vs. β, a good correlation was found, linear regression yielding $\Delta\bar{R}/\Delta t = 1.04\beta$. This means that $\Delta\bar{R}/\Delta t$ and β can be used alternatively as practically equivalent measures of the spreading kinetics.

The decay in the through-penetration of Ga in Fig. 3b is another manifestation of this "freak" wetting behavior. Its exact origin is not clear at the moment; it may be related to contamination imposed on the soft Ag by the small sharp wood sticks used in our experiments for placing the Ga drops on the Ag/glass substrate, to formation of air/water pockets, to residual stress or to plastic strain. Note that this decay in through-penetration at the center of the drop did not prevent accurate measurements of the extension rate $\Delta R/\Delta t$ of the drop perimeter.

Fig. 9 shows that the spreading of Ga was faster as temperature was raised. These experiments were performed by means of the "one drop/many temperatures" technique, as follows. A Ga drop was placed on the Ag film at 0 °C for 100 min, and the spreading kinetics was monitored. The

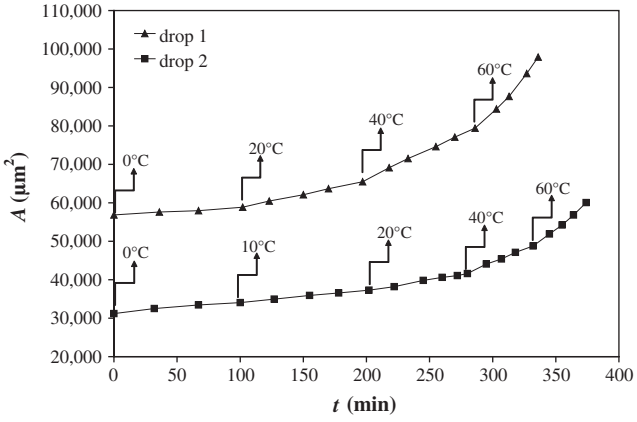

Fig. 9. Time dependence of the drop area A, as revealed by ODMT experiments. Drops 1 and 2 had initial areas A_0 = 57,000 and 31,000 μm^2, respectively. Arrows note the time at which the exposure temperature was raised (the new temperature value is also noted).

temperature was then raised to 10 °C, and the kinetics at this new temperature was monitored for additional 100 min. The procedure was repeated, increasing the temperature to as high as 60 °C. Several conclusions can be drawn from Fig. 9. First, the spreading rate increased with temperature, thus suggesting a thermally activated process. Second, spreading occurred at temperatures as low as 10 °C, i.e. below the melting point of pure Ga or the Ga–Ag eutectic. Light microscopy observations confirmed that in these experiments with non-precooled (npc) Ga, the drop at 10 °C was in the liquid state. Additional experiments were performed in order to learn whether penetration and spreading of Ga could occur when Ga was in the solid-state after precooling to well below its melting temperature. To this end, liquid drops of Ga were placed on the Ag film, and the whole Ga/Ag/glass sandwich was immediately deep-frozen at $T = -78$ °C in liquid acetone cooled by dry ice. The spreading kinetics was subsequently monitored at different temperatures in the range from −10 to +60 °C, and the spreading rate $\Delta\bar{R}/\Delta t$ measured for these precooled (pc) samples.

Surprisingly, it was observed that spreading and through-penetration can occur even in the pc samples quenched at −78 °C, a temperature well below the melting point of Ga. In these samples we found fairly good correspondence between the top and bottom views of the spreading front and extension of the grey region around the bulk drop. The behavior of the pc samples is compared to that of the npc samples in Fig. 10. Above the melting point of Ga, the pc and npc samples naturally feature the same spreading/penetration rate $\Delta R/\Delta t$, and the activation energy of the process, as obtained from Fig. 10, is $E_L = 28.9 \pm 4.8$ kJ mol^{-1}. This value is compatible with the typical activation energy of diffusion in liquid metals and alloys and is well below the value typical of GB diffusion in Ag. In contrast, below the melting point of Ga, the kinetics data for the pc samples are heavily scattered – some of the pc samples show $\Delta\bar{R}/\Delta t$ comparable to that for their npc counterparts, while others feature a much smaller and hardly measurable velocity $\Delta R/\Delta t < 1.7 \times 10^{-16}$ m s^{-1}, i.e. they show no visible extension of the grey area. The origin of such a behavior could be due to large internal stress caused by quenching the Ga/Ag/glass sandwich at −78 °C. This issue will be discussed in Section 4. The straight line 2 in Fig. 10 is drawn through the points for which $\Delta R/\Delta t$ still could be measured, ignoring the points that fall on the npc line and are shown separately. The slope of line 2 yields $E_S = 48.2 \pm 9.6$ kJ mol^{-1}. Fig. 10 shows that, close to the melting point of Ga, the spreading rate $\Delta R/\Delta t$ for the npc samples wetted with liquid Ga is about three times that of the pc samples.

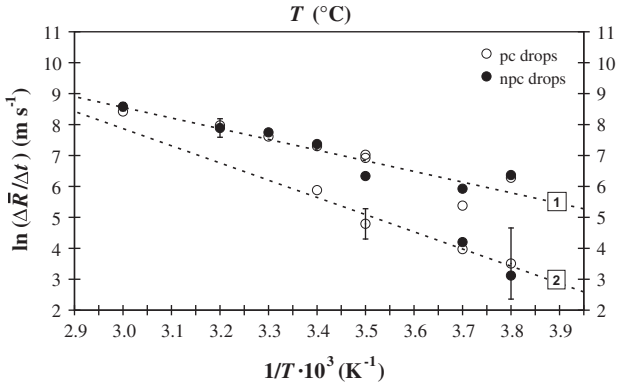

Fig. 10. Temperature dependence of the linear spreading rate $\Delta\bar{R}/\Delta t$ of the grey region. Filled circles (1, npc samples): the Ag–Ga samples were held at $-10\ °C \leqslant T \leqslant 60\ °C$, where Ga was expected to be liquid. Open circles (2, pc samples): the samples quenched at −78 °C were held at $-10\ °C \leqslant T \leqslant 21\ °C$, i.e. below the melting point of the Ga–Ag eutectic, where Ga was expected to be solid.

4. Discussion

4.1. Kinetic regime of spreading

It seems likely that the capillary forces decelerate when the contact angle reaches some stationary value. Further spreading is slower and can be controlled by attachment/detachment processes at the triple "solid–liquid–vapor" junction rather than by viscous flow. By analogy with formal chemical kinetics, this interface reaction-controlled regime can be called "kinetic" to distinguish it from the "transport", i.e. purely hydrodynamic regime of viscous flow, or "molecular-dynamic controlled" in the terminology of Saiz and Tomsia [22]. To meet the continuity, the viscous flow flux, J_{VF}, towards a triple junction should be coupled with the "interface reaction" flux, J_R, directed into the virgin region. The hump formed at the moving front of the grey region (Fig. 6e) helps in providing the coupling in the situation when an outcome reaction flux J_R in itself is smaller than the hydrodynamic flux J_{VF}. An analogy here is the increase in the pressure of a liquid in a narrow section of the tube with periodic variations in its cross-section.

The onset of the grey region in our experiments can likely be attributed to transition to a "kinetic" regime of spreading, with constant velocity $v = \Delta R/\Delta t \approx 10^{-9}$ m s^{-1} at RT and activation energy 28.9 kJ mol^{-1} (see Fig. 10, line 1). Within this approach, the contact angle $\theta \approx 30°$ could be interpreted as a stationary, or slowly decreasing, value rather than an equilibrium one. With the aforementioned $v \approx 10^{-9}$ m s^{-1}, the surface energy of liquid Ga, $\gamma_{LV} = 0.7$ J m^{-2}, and its viscosity $\eta_{Ga} \approx 1.7 \times 10^{-3}$ Pa s at 27 °C [26], the capillary number, Ca_{300}, is [22]:

$$Ca_{300} = v\eta_{Ga}/\gamma_{LV} \approx 3 \times 10^{-12} \quad (6)$$

The maps "contact angle θ vs. Ca" for the kinetic regime of spreading of a uniform liquid layer over a flat substrate were constructed for several liquid/solid metal systems in Ref. [22]. According to these maps (see Fig. 3b in Ref. [22]), $\theta \approx 30°$ corresponds to $Ca \approx 10^{-4}$–10^{-3}. For correct comparison with the $Ca_{300} \approx 3 \times 10^{-12}$ obtained from Eq. (6), one should note that the maps in Ref. [22] were constructed based on wetting experiments performed at

1100 °C, while the work reported herein was conducted at around 27 °C. To correct for temperature, we used the activation energy of spreading in the "kinetic" or "molecular-dynamic controlled" regime $\Delta G_W = 96.5$ kJ mol^{-1}, which yielded the best fit to the experimental data in Ref. [22], and calculated the ratio $v_{1373}/v_{300} = \exp(-\Delta G_W/1373k_B)/\exp(-\Delta G_W/1073k_B) = 3 \times 10^{13}$. With this correction factor, and ignoring a weak temperature dependence of the group $(\eta_{Ga}/\gamma_{LV}) \approx 10^{-3}$ s m^{-1} in Eq. (6), extrapolation of $Ca \approx 10^{-4} \div 10^{-3}$ to 27 °C yields $Ca_{300} = 10^{-4} \div 10^{-3}/3 \times 10^{13} \approx 10^{-17}$. The extrapolated velocity that corresponds to this extrapolated Ca_{300} is $v_{300} \approx 10^{-14}$ m s^{-1}, while the experimental value is $v_{300} \approx 10^{-9}$ m s^{-1}. Note that for $\theta < 30°$, which is possible in the extension of a thin precursor film, this striking difference between the spreading rates will be even higher. This discrepancy shows that extension of the grey region in our experiments at RT occured much faster compared to that expected in Ref. [22] for a kinetic regime of spreading over a flat substrate. Together with the linear spreading (Fig. 7) that supported just the kinetic regime, this finding suggests the presence of surface defects which affected surface roughness in such a way that it promoted spreading. We propose that GB grooves play the major role among these defects and that spreading occurs via "secondary wetting". Another important argument against the idea that the synchronized spreading in the "kinetic" regime occurred over a flat surface is obviously the dramatic difference between the activation energy $E_L \cong 28.9 \pm 4.8$ kJ mol^{-1} found for this process in our experiments and the value $\Delta G_W = 96.5 \pm 9.7$ kJ mol^{-1} suggested in Ref. [22].

4.2. Secondary wetting

The extension of a lusterless "grey" spot around a static drop of wetting liquid metal (Hg, Ga, Sn, etc.) placed onto the surface of various polycrystalline metals have been discussed extensively for decades in terms of various mechanisms of surface diffusion or/and wetting [24,25,27,28]. Nowadays, it is widely presumed that this phenomenon results from a so-called secondary wetting attributed to the promotion of wetting by GB grooves [24].

Grain boundary grooving (GBG) is a spontaneous process driven by the tendency to minimize the total surface and GB energy, and is controlled by the rate of capillary-driven diffusion mass transport [29]. Thermal GB grooves in polycrystalline metals form even in vacuum [29], but their formation is particularly fast in the presence of wetting liquid metals [30–32]. In this case, spreading of liquid metals can continue by flowing along the GB channels which radiate from the macroscopic triple line [24,25,28,33]. Summ and Gorynov [25] provided good evidence in support of this mechanism. These authors observed extension of the lusterless, "grey" region ahead of an Hg drop on the surface of Zn polycrystals. They confirmed by autoradiography the presence of the network of GB grooves infiltrated with Hg and showed finally that the grey region did not form at the surface of a Zn single crystal. Later, Sharps et al. [33] studied the secondary wetting of a Cu–Ag solid solution with small (20 μm) grains by a liquid eutectic Ag–Cu. They observed the formation of a dense network of GB liquid channels ahead of the triple junction, resulting in a macroscopic dihedral angle θ nearly equal to zero. When the liquid fills the GB channels, it can also expand onto the free surface on both sides of the grooves, forming liquid caps having their bases in the grooves. The width of the caps scales with the groove depth and increases with time, so that they can merge [24]. The spreading of the thus-formed film will be controlled by the grooving rate.

We propose that the common process that controls both the lateral spreading and through-penetration of Ga in our experiments, and is responsible for the observed perfect matching of the top and bottom views of the film, is just secondary wetting. According to this mechanism, the spreading rate v of the moving grey front is determined by the groove extension rate v_{GBG}; the latter is much the same in the lateral and vertical directions. Grain boundary diffusion of Ga into solid Ag and the formation of an IMC between Ag and Ga complicate the analysis; we will therefore attempt to clarify the role of these factors. Regarding dissolution of Ag into liquid Ga, this process could not occur in our experiments due to the aforementioned presaturation of Ga with Ag.

4.3. Spreading mechanism: grain boundary diffusion, intermetallic formation or grooving?

The activation energy for the penetration/spreading of liquid Ga on Ag, $E_L \cong 28.9$ kJ mol^{-1}, is considerably smaller than can be expected for any solid-state diffusion process in Ag [34], but is comparable with an activation energy of diffusion in liquid metals and alloys [26,34]. The measured value of the activation energy for the penetration/spreading of solid Ga on Ag, $E_S = 48.2$ kJ mol^{-1} (Fig. 10, line 2), also seems to be too small for solid-state processes in Ag. For example, GB self-diffusion of Ag shows activation energy $E = 72.4$ kJ mol^{-1} [34], whereas GB diffusion of indium (an element which belongs to the IIIA group of the periodic table, like Ga) in Ag shows $E = 61.7$ kJ mol^{-1} [34].

As was already mentioned, the penetration of Ga through the Ag film with thickness $h \approx 0.47$ μm takes approximately 25 s at RT. Assuming a constant penetration rate, one obtains its mean value, $v_p \approx 19$ nm s^{-1}. The diffusion rate v_p is of the order of D/h, and with this we get the rough estimate $D_{Ga} = h\, v_p \approx 10^{-12}$ m s^{-1}. The diffusivity of Ga in GBs of Ag has not been reported, but it should, in principal, not differ much from that of In in GBs of Ag. Yet, at RT, the latter was reported to be only $D \leqslant 7 \times 10^{-17}$ m^2 s^{-1} [34], which is much lower than D_{Ga}.

The rapid penetration observed may, in principle, be related to formation of IMCs between Ag and Ga; our EDS observations suggest that IMCs may have actually

formed in the grey region. However, if the IMCs form and Ga diffuses preferably through these IMC films, would the process be rapid? The strong chemical bonds in IMCs should result in higher activation energies for diffusion compared to those in pure metals. For example, the GB diffusion of Ga or Ni in Ni_3Ga shows an activation energy of $\sim$183.3 kJ mol^{-1} [35]. Therefore, the formation of Ag_3Ga cannot explain the fast penetration/spreading kinetics, and is assumed to represent a secondary process which follows fast GB grooving, the penetration mechanism that is discussed in detail below. We assume that formation of a continuous IMC layer either does not occur or requires more time than GB grooving via dissolution and diffusion through liquid, so that IMC does not prevent Ag from intimate contact with liquid Ga. The literature on soldering shows that in many cases the layers of IMCs formed are not actually continuous but have the scallop-type morphology, so that the liquid metal has easy access to the solid one. Particularly interesting are the recent observations by Tu et al. [36], which showed that when the molten solder reacts with the layer-type IMC, the reaction begins by wetting high-angle GBs in the IMC by the solder, a process that follows at GBs of the solid metal substrate. Tu et al. noted that the scalloped morphology of the IMC enables a high rate of exothermal wetting reaction.

Assuming that GB diffusion of Ga and formation of IMC occurred in the solid Ag, one can expect that the rate of the penetration/spreading would be the same with liquid and solid Ga as the diffusants. In contrast to this, Fig. 10 clearly shows that the penetration/spreading rate is considerably faster with liquid Ga. The diffusion coefficient D_L for liquid-phase diffusion in metals is many orders of magnitude higher that for solid-phase diffusion [11,12,34], and fast diffusion through liquid seems to be the actual process that controls the fast spreading and penetration. The observation of grain coarsening (Fig. 5) may be considered as evidence in support of this idea, because the presence of a liquid metal between grains is known to accelerate grain growth [19] and GBG [29–32] dramatically. Our hypothesis is that the secondary wetting outside the black region becomes possible because of the formation of GB grooves filled with liquid Ga. The exact matching between the top and bottom views of the grey region is thought to result from the formation and extension of such grooves filled with Ga. The GB grooves reach the interface between the tiny grained Ag film and the glass substrate, and form a dense, hatched network there, which appears under a light microscope as a "grey region".

4.4. Morphology of grain boundary grooves formed in Ag in the presence of liquid Ga

According to this mechanism, the spreading rate v of the moving grey front is determined by the groove extension rate v_{GBG}; the latter is much the same in the lateral and vertical directions. Grooves formed during the wetting process increase the actual area of the solid/liquid interface and, therefore, provide better thermodynamic conditions for wetting, which can occur when the following criterion is met [24,25]:

$$\gamma_{GB}/2\gamma_{SL} = \cos\theta/2 \geqslant \sin\theta_0 \tag{7}$$

where θ_0 is the wetting angle formed by the drop on the macroscopically smooth solid surface and

$$\theta = 2\cos^{-1}(\gamma_{GB}/2\gamma_{SL}) \tag{8}$$

is the contact angle at the groove tip that is dictated by the equilibrium between the GB surface tension γ_{GB} and the surface tension γ_{SL} of the interface between liquid Ga and solid Ag. The larger the wetting angle θ_0 (or, in other words, the poorer the wettability is), the smaller should be θ at the tip of the groove to allow secondary wetting. Our observations showed that, for Ga on Ag, $\theta_0 \cong 30^\circ$ and, with this, Eq. (7) predicts that the wetting is possible at $\theta \leqslant 120^\circ$. This is not a strict requirement. Indeed, a dihedral angle θ of about 120–150° is typical for the thermal grooves formed at a random high-angle GB in vacuum [29], while γ_{SV} at the solid–vacuum interface is always larger compared to γ_{SL}; this means that the θ formed in the presence of a liquid metal will be smaller than 120°. With the realistic values $\gamma_{GB} \cong 0.5$ J m^{-2} for Ag and $0.3 \leqslant \gamma_{SL} \leqslant 0.4$ J m^{-2}, Eq. (8) predicts $67^\circ \leqslant \theta \leqslant 103^\circ$. This is quite a large dihedral angle that allows easy penetration of liquid Ga to the tip of an advancing groove without a steric barrier.

4.5. Grooving and spreading kinetics

4.5.1. Grooving assisted by liquid Ga

As mentioned above, the exact matching between the top and bottom views of the grey region results, in our view, from a dense network of GB grooves filled first with liquid Ga (and later with IMC), which reaches the Ag/glass interface. The spreading/penetration rate in this model is determined by the GB grooving rate.

According to Mullins [29] and Robertson [32], the depth of the groove ΔL increases with time t as:

$$\Delta L \approx ctg(\theta/2)(Ct)^{1/3} \tag{9}$$

where the constant C depends only on the material properties in the solid/liquid couple:

$$C = D_L c_{\infty L}\gamma_{SL}\Omega/k_B T \tag{10}$$

Here, D_L is the diffusion coefficient of solid Ag in liquid Ga, $c_{\infty L}$ is the equilibrium solubility (atomic fraction) of solid Ag in liquid Ga, Ω is the atomic volume of Ag, k_B is the Boltzmann constant and T is temperature. From Eq. (9) it follows that the time $t^* \propto h^3$ required for groove penetration through the film thickness h, that is from $\Delta L = 0$ or $\Delta L = h$, defines the average grooving velocity:

$$v_{GBG} = h/t^* \tag{11}$$

Eqs. (9) and (11) yield:

$$v_{GBG} = C/h^2 \cdot [tg(\theta/2)]^3 \quad (12)$$

We propose that the GBG process, assisted by very fast liquid-phase diffusion, is responsible for both penetration and spreading, which result from the simultaneous extension of the same GB grooves in both the normal and lateral directions. Thus, the experimental linear spreading velocity $\Delta R/\Delta t$, or β, equals essentially the grooving velocity given by Eq. (12).

Let us estimate how large should be the diffusion coefficient D_L of Ag in liquid Ga to fit the observed $\Delta R/\Delta t = 1.5 \times 10^{-9}$ m s^{-1} at 20 °C (Fig. 10, line 1). Substituting $T = 293$ K, $c_{\infty L} = 2 \times 10^{-4}$ (eutectic in Fig. 1), $\gamma_{SL} = 0.34$ J m^{-2}, $\Omega = 10^{-29}$ m^3, $h = 4.7 \times 10^{-7}$ m and $\theta = 85°$ into Eq. (12), one obtains $D_L = 2.6 \times 10^{-9}$ m^2 s^{-1}. This value is reasonable for diffusivity in liquid metals; D_L for self- and hetero-diffusion is typically $\sim 10^{-9}$ m^2 s^{-1} [11,12,26,34] when the components of the liquid do not form chemical compounds [26]. Hence, we conclude that the groove-assisted wetting is fast enough to account for the observed penetration/spreading rate.

It is worth noting also that the $E_L \cong 28.9$ kJ mol^{-1} found from our spreading experiments is typical of many solder wetting reactions [11,12], but is larger than the specific value of 4.8 kJ mol^{-1} reported in Ref. [26] for self-diffusion in liquid Ga. It seems likely that the higher activation energy and the smaller diffusivity D_L mentioned result from the same factor – chemical interaction between Ga and Ag in the liquid. It is known that chemical interaction between constituents, in particular at the composition of a liquid alloy that is close to the IMC composition, often results in considerable reduction in D_L and increase in E_L [34]. It is also possible that the detachment and attachment reactions at the solid Ag (or IMC)–liquid Ga interface involved in GBG increase the activation energy of GBG above E_L and thus cause a decrease in the effective diffusivity. The very short diffusion distances involved in GBG in the 0.47 μm Ag thin film favor this possibility of a mixed "diffusion/reaction" grooving regime.

4.5.2. Grooving assisted by solid Ga

It is known that GBG and wetting can also occur in "solid/solid" metal couples [37,38]. This is so in particular when the diffusion mobility in one of the metals, say "A", is much higher than in another metal, so that "A" can act as a fast diffusion pathway, in this respect playing the role of the liquid phase in liquid–solid couples. We have suggested elsewhere [39] that GBG assisted by solid Ga operates in precooled Ag–Ga samples, below the melting temperature (Fig. 10, line 2). Residual stress in solid Ga, which can form due to structural misfit at the solid Ga/Ag interface, is expected to be completely released, as the Ga in our experiments is very close to its melting point. This suggests that the interfacial energy γ_{SL} is dictated in this case mainly by its chemical component, and should be close to that at the liquid Ga/Ag interface. We assumed further that diffusion of Ag atoms out of the growing groove occurred along GBs of solid Ga. We applied Eqs. (10) and (12), in which instead of D_L we used the product $D_{GB}(\delta/d)$, with D_{GB} being the GB diffusion coefficient of Ag in solid Ga at RT, δ the GB thickness and d the grain size in solid Ga.

Substituting $D_{GB}(\delta/d)$ for D_L and using the reasonable values $d = 10^{-6}$ m, $\delta = 5 \times 10^{-10}$ m, $\gamma_{SL} \cong 0.3$ J m^{-2} and $\theta = 70°$, it is found from Eq. (12) that it fits the experimental spreading velocity $(\Delta R/\Delta t) = 7 \times 10^{-10}$ m s^{-1} (Fig. 10, line 2 at $T = 30$ °C) at $D_{GB} \approx 2 \times 10^{-9}$ m^2 s^{-1}. For most solid metals, the GB diffusion coefficient D_{GB} near the melting temperature is of the order of 10^{-9} m^2 s^{-1} [14], thus indicating fairly good agreement between the theory and experimental data. Furthermore, the measured $E_S \cong 48.2$ kJ mol^{-1} (Fig. 10, line 2) can be reproduced in the solid-state grooving model and attributed to the activation energy of GB diffusion in solid Ga, E_{GB}^{Ga}. While the experimental value of E_{GB}^{Ga} is not known, we estimate it roughly, as described below.

The stable phase of Ga under normal conditions is orthorhombic, with eight atoms in the conventional unit cell. Each atom has only one nearest neighbor and the bonding between atoms is covalent, hence the Ga_2 dimer is seen as the fundamental building block of the crystal. Strong atomic bonds in the dimers are responsible for the high boiling point (2204 °C), while weak secondary bonds between dimers dictate the extremely low melting point. Considering high-angle GBs in Ga as a disordered "phase" in which diffusional mobility is determined by the secondary bonds, the activation energy of Ga self-diffusion in this GB "phase" can be roughly estimated by the well-known empirical relation $E_{GB}^{Ga} \approx 18 k_B T_m$ [34]. This estimate yields $E_{GB}^{Ga} \approx 48.2$ kJ mol^{-1}. One should not expect a dramatic difference between E_{GB} for GB self-diffusion of Ga and that for GB hetero-diffusion of Ga in Ag [40].

4.6. On the role of thermal stress

The data in Fig. 10 stimulate the question why some of the Ag films exposed below the melting point of Ga to "precooled", expectedly solid, Ga show high penetration/spreading rate, which is typical of liquid Ga at temperatures above its melting point, while some nominally similar samples showed a very slow, unmeasurable, spreading/penetration rate. This "freak" behavior may be related to the fact that Ga expands on solidification, showing a volumetric change $\Delta V/V_0 = +3.2\%$ at T_m(Ga) and pressure $P = 1$ atm (see Table 1).

In order to quantify such a behavior, let us assume that a small "inclusion" of liquid Ga that penetrated at GBs of solid Ag is surrounded by a strong IMC or is otherwise perfectly constrained against free expansion under solidification. In this case of perfect three-dimensional (3-D) constraint, the 3.2% volumetric expansion of Ga under solidification forms in the inclusion under very high hydrostatic compression stress, ΔP:

$$\Delta P = K(\Delta V/V_S) = 0.032K \approx 2.1 \text{ GPa} \quad (13)$$

Table 1
Materials parameters used in the calculation of the change of the melting point under pressure.

Metal	Atomic volume ($\Omega \times 10^{17}$ m^3)	Volume change due to fusion, $\Delta V/V_S = (V_S - V_L)/V_S$	Bulk modulus, K (GPa)	Normalized entropy of fusion, S_F/k_B [26,41]	Surface energy of liquid, γ_{LV} (J m^{-2}) [26]	Melting temperature T_{m0} at ambient pressure, P_0 (K)
Ga	2	+0.032	67	2.3	0.74	303
Bi	3.8	+0.034	37	2.3	0.38	544
Solid Ag	2	−0.038	76	1.1	0.87	1234

Subscripts S and L refer to the solid and liquid states, respectively.

where $K = 67$ GPa is the bulk modulus of Ga (Table 1). The pressure makes solidification more difficult, increases the stability of the low-volume liquid Ga phase and thus shifts the equilibrium solidification/melting point T_m to a lower temperature, by ΔT_m. The value ΔT_m can be estimated from the Clapeyron equation [42,43]:

$$\Delta T_m = \Delta V \Delta P / S_F \quad (14)$$

where S_F is the entropy of fusion, given in Table 1. Eqs. (13) and (14) yield:

$$\Delta T_m = (\Delta V)^2 K / V_S S_F = 49^\circ \quad (15)$$

Along with the approximate estimation from Eqs. (13) and (14), one can use the experimental P–T phase diagram for Bi [42,43] to get an idea on how large ΔT_m should be for Ga. The use of the Bi diagram here is justified since Bi has the same entropy of fusion, S_F, as Ga and practically the same positive change in the molar volume, $\Delta V/V_S$, on solidification (see Table 1). Moreover, the behavior of Bi under high pressure has been studied more than that of Ga, which shows a number of metastable phases in the P–T phase diagram, e.g. melts at RT at $P \approx 2$ GPa, and crystallizes again in the metastable phase Ga-III with further increase in P [44]. The bulk modulus of Bi is smaller than that of Ga (Table 1), hence Eq. (15) predicts a reduction in ΔT_m. In spite of this, the P–T diagram for Bi reproduced in Refs. [42,43] shows $\Delta T_m = 102^\circ$ under the same compression stress $P = 2$ GPa that has been estimated to act on the perfectly constrained Ga inclusion. We can conclude here that 3-D constrained liquid particles of Ga under liquid–solid transformation experience high hydrostatic pressure and will therefore solidify at 50–100° below the melting point at ambient pressure, T_m(Ga) ≈ 29.8 °C. This effect has thermodynamic origin and does not relate directly to the well-known kinetic overcooling of liquid Ga.

Note that the pressure $\Delta P \approx 2.1$ GPa found from Eq. (13) is the maximum pressure in the Ga inclusion under perfect 3-D constraint. If, however, the constraint to free volumetric expansion ΔV can be relieved, say by delamination of the Ag film from the glass substrate, bulging the film, crack formation or Ga egress on the surface, Ga will become solid after precooling at −78 °C; in this case, the spreading rate will be that characteristic of solid Ga and the points in Fig. 10 should fall on line 2. Real Ga inclusions are likely embedded at GBs, grooves and microcracks, and may have a wide spectrum of constraints and, thus, of melting temperatures. This expectation corresponds to the data by Di Cicco [45], who observed that isolated micrometer-sized Ga drops embedded in a mixture of LiF and epoxy show a wide range of melting points under a fixed pressure of the order of several gigapascals.

Even under 2-D constraint, which can be caused merely by adhesion of a cake-like Ga drop to the Ag film, a large compressive stress, of the order of $\sigma \approx E(\Delta V/V_S)$, with $E \approx K$ being Young's modulus of elasticity, forms in the drop upon quenching at −78 °C. This stress acts in the plane parallel to the Ag–Ga interface, and can cause either reduction in the melting point T_m or, when the adhesion of the drop to the Ag film is weak, buckling of the Ga cake and its detachment from Ag. In the latter case, spreading/penetration of Ga can no longer occur. To summarize, it seems likely that the high thermal stress generated in our experiments with precooled samples is responsible for the freak behavior observed in Fig. 10. This is because some of the Ga drops can detach from Ag under this stress, while others remain liquid after precooling and subsequent heating.

5. Conclusions

The following conclusions can be drawn:

(1) The synchronized surface spreading and through-penetration of liquid and solid Ga on polycrystalline Ag thin films, as observed for the first time in this work, are likely controlled by a common mechanism.
(2) Linear spreading with activation energies $E_L \cong 28.9 \pm 4.8$ kJ mol^{-1} and $E_S \cong 48.2 \pm 9.6$ kJ mol^{-1} for liquid and solid Ga, respectively, was observed. Neither formation of an intermetallic compound nor GB diffusion of Ga in Ag determined the rate of the process.
(3) Grain boundary grooving, with Ag diffusion out of the groove either through liquid Ga or solid Ga, is a possible mechanism of the spreading and penetration.
(4) The model proposed herein reproduced the observed spreading/penetration rates and gave reasonable estimates of the energies E_S and E_L.
(5) Additional experimental work is required to verify the proposed grooving model. In particular, penetration experiments on thin films of different thicknesses may be helpful.
(6) The observed through-penetration of a metal with low melting point in either liquid or solid-state may have important implications in failures of thin metal film parts joined with lead-free solders in the microelectronic industry.

References

[1] Glickman EE, Nathan M. J Appl Phys 1999;85:3185.
[2] Glickman EE. In: Lépinoux J, Mazière D, Pontikis V, Saada G, editors. Modeling & materials engineering, NATO sciences series E. Multiscale phenomena in plasticity: from experiments to phenomenology, vol. 367. Dordrecht: Kluwer Academic Publishers; 2000. p. 383.
[3] Marie MN, Wolski K, Biscondi M. Scr Mater 2000;43:943.
[4] Pereiro-López E, Ludwig W, Bellet D. Acta Mater 2004;52:321.
[5] Chatain D, Rabkin E, Derenne J, Bernardini J. Acta Mater 2001;49:1123.
[6] Lynch SP. Mater Charact 1992;28:279.
[7] Vogel H, Ratke L. Acta Metall Mater 1991;39:641.
[8] Rabkin E. Scr Mater 1998;39:685.
[9] Glickman E. Z Metallk 2005;96:1204.
[10] Vilenkin A. Defect Diff Forum 2003;216–217:189.
[11] Tu KN. Solder joint technology: materials, properties and reliability. New York: Springer; 2007. p. 387.
[12] Ohring M. Reliability and failure of electronic materials and devices. San Diego, CA: Academic Press; 1998. p. 692.
[13] Zhang Y, Li JB, Liang JK, Liu QL, Xiao YG, Zhang Q, et al. Comput Coupling Phase Thermochem 2006;30:316.
[14] Okamoto H. J Phase Equilib Diff 2008;29:111.
[15] Hansen M, Anderko K. Constitution of binary alloys. New York: McGraw-Hill; 1958. p. 606.
[16] Ina K, Koizumi H. Mater Sci Eng A 2004;387–389:390.
[17] Kodama Y, Choi PK, Koizumi H, Hyodo S. Mater Sci Eng A 1994;176:231.
[18] Tanaka R, Choi PK, Koizumi H, Hyodo S. Mater Trans 2001;42:138.
[19] German RM. Liquid phase sintering. New York: Plenum Press; 1985. p. 380.
[20] Dubrovskii VG, Sibirev NV, Cirlin GE, Harmand JC, Ustinov VM. Phys Rev E 2006;73:021603.
[21] Eustathopoulos N. Acta Mater 1998;46:2319.
[22] Saiz E, Tomsia A. Nature Mater 2004;3:903.
[23] Saiz E, Tomsia A, Cannon R. Acta Mater 1998;46:2349.
[24] Eustathopoulos NN, Nicholas MG, Drevet B. Wettability at high temperatures. Oxford: Pergamon Press; 1999. p. 428.
[25] Summ BD, Gorynov Yuv. Physico-chemical basis of wetting and spreading. Moscow: Khimia; 1976. p. 232 [in Russian].
[26] Wilson DR. Structure of liquid metals. London: Institute of Metals; 1965. p. 202.
[27] Heumannn Th, Forch K. Z Metallk 1962;53:122.
[28] Buhovskii AI. Spreading. Kiev: Naykova dymka; 1983. p. 191 [in Russian].
[29] Mullins WW. J Appl Phys 1957;28:333.
[30] Mullins WW. Trans Metall Soc AIME 1960;218:354.
[31] Allen BC. Trans Met Soc AIME 1966;236:915.
[32] Robertson WM. Trans Met Soc AIME 1965;233:1232.
[33] Sharps P, Tomsia A, Pask J. Acta Metall 1982;29:855.
[34] Kaur I, Gust W, Kozma L. Handbook of grain and interphase boundary diffusion data, vol. I. Stuttgart: Ziegler Press; 1989. p. 720.
[35] Cermack V, Rothova V. Intermetallics 2002;10:765.
[36] Tu N, Gusak AM, Li M. J Appl Phys 2003;93:1335.
[37] Straumal B, Baretzky B. Defect Diff Forum 2003;217–217:53.
[38] Josell D, Spaepen F. In: Nix WD, Bravman JC, Arzt E, Freund LB, editors. MRS symposium proceedings, vol. 239. Pittsburgh, PA: Materials Research Society; 1992. p. 515.
[39] Glickman E, Levenstein M, Budic L, Eliaz N. Defect Diff Forum 2006;249:219.
[40] Kaur I, Gust W. Fundamentals of grain and interphase boundary diffusion, vol. II. Stuttgart: Ziegler Press; 1989. p. 424.
[41] Sawamura H. Trans JIM 1972;13:225.
[42] Swalin R. Thermodynamics of solids. New York: John Wiley; 1962. p. 302.
[43] Machlin ES. An introduction to aspects of thermodynamics and kinetics relevant to materials science. New York: Giro Press; 1991. p. 343.
[44] Degtyareva O, McMahon M, Nelms R. Acta Cryst 2002;A58(Suppl. C): 175.
[45] Di Cicco A. Phys Rev Lett 1998;81:2942.